

# High-field superconductivity in alloyed MgB<sub>2</sub> thin films

V. Braccini<sup>1</sup>, A. Gurevich<sup>1</sup>, J.E. Giencke<sup>1</sup>, M.C. Jewell<sup>1</sup>, C.B. Eom<sup>1</sup>, D.C. Larbalestier<sup>1</sup>, A. Pogrebnnyakov<sup>2</sup>,  
Y. Cui<sup>2</sup>, B. T. Liu<sup>2</sup>, Y. F.Hu<sup>2</sup>, J. M. Redwing<sup>2</sup>, Qi Li<sup>2</sup>, X.X. Xi<sup>2</sup>, R.K. Singh<sup>3</sup>, R. Gandikota<sup>3</sup>, J. Kim<sup>3</sup>, B.  
Wilkins<sup>3</sup>, N. Newman<sup>3</sup>, J. Rowell<sup>3</sup>, B. Moeckly<sup>4</sup>, V. Ferrando<sup>5</sup>, C. Tarantini<sup>5</sup>, D. Marré<sup>5</sup>, M. Putti<sup>5</sup>, C.  
Ferdegini<sup>5</sup>, R. Vaglio<sup>6</sup>, E. Haanappel<sup>7</sup>

<sup>1</sup>*Applied Superconductivity Center, University of Wisconsin – Madison, WI*

<sup>2</sup>*Pennsylvania State University, University Park, PA*

<sup>3</sup>*Arizona State University, Tempe, AZ*

<sup>4</sup>*Superconductor Technologies Inc, Sunnyvale, CA*

<sup>5</sup>*University of Genoa / INFN-LAMIA, Genoa, Italy*

<sup>6</sup>*University of Naples / INFN-Coherentia, Naples, Italy*

<sup>7</sup>*Laboratoire National des Champs Magnétiques Pulsés, CNRS-UPS-INSA, Toulouse, France*

We investigated the effect of alloying on the upper critical field  $H_{c2}$  in 12 MgB<sub>2</sub> films, in which disorder was introduced by growth, carbon doping or He-ion irradiation, finding a significant  $H_{c2}$  enhancement in C-alloyed films, and an anomalous upward curvature of  $H_{c2}(T)$ . Record high values of  $H_{c2}^{\perp}(4.2) \approx 35\text{T}$  and  $H_{c2}^{\parallel}(4.2) \approx 51\text{T}$  were observed perpendicular and parallel to the *ab* plane, respectively. The temperature dependence of  $H_{c2}(T)$  is described well by a theory of dirty two-gap superconductivity. Extrapolation of the experimental data to  $T=0$  suggests that  $H_{c2}^{\parallel}(0)$  approaches the paramagnetic limit of  $\sim 70\text{T}$ .

Discovery of superconductivity in  $\text{MgB}_2$  with the critical temperature  $T_c = 39\text{K}$  renewed intense interest in the novel effects in two-gap superconductors. *Ab initio* calculations<sup>1,2</sup> showed that  $\text{MgB}_2$  has two weakly coupled gaps  $\Delta_\sigma(0) \approx 7.2\text{meV}$  and  $\Delta_\pi(0) \approx 2.3\text{meV}$  residing on disconnected sheets of the Fermi surface formed by in-plane  $p_{xy}$  boron orbitals ( $\sigma$  band) and out-of-plane  $p_z$  boron orbitals ( $\pi$  band). The two-gap Eliashberg theory<sup>2,3</sup> has explained many anomalies in tunneling, heat capacity and electrostatics of clean  $\text{MgB}_2$  single crystals.<sup>4</sup> However, the physics of two-gap  $\text{MgB}_2$  alloys determined by the multiple impurity scattering channels, and by the complex substitutional chemistry of  $\text{MgB}_2$ <sup>5</sup> are still poorly understood. The behavior of disordered  $\text{MgB}_2$  is particularly interesting because it exhibits enormous enhancement of  $H_{c2}$  by nonmagnetic impurities,<sup>6-8</sup> well above the estimate  $H_{c2}(0)=0.69T_cH'_{c2}(T_c)$  of one-gap theory<sup>9</sup>, and anomalous temperature-dependent  $H_{c2}$  anisotropy.<sup>4</sup> Some of these features have been recently explained by generalized two-gap Usadel equations<sup>10,11</sup> in which impurity scattering is accounted for by the intraband electron diffusivities  $D_\sigma$  and  $D_\pi$ , and interband scattering rates  $\Gamma_{\sigma\pi}$  and  $\Gamma_{\pi\sigma}$ . In this Letter we present high-field transport measurements of  $H_{c2}(T)$  for 12  $\text{MgB}_2$  films made by 6 different groups using very different ways of introducing disorder. We show that  $H_{c2}$  is radically increased in dirty films, and  $H_{c2}^{\parallel}(0)$  extrapolates to  $H_p \sim 70\text{T}$  for a C-alloyed film, comparable to the paramagnetic limit ( $H_p=1.84T_c = 64\text{T}$  for  $T_c = 35\text{K}$ ).

Our films were made by different deposition techniques including pulsed laser deposition (PLD),<sup>12,13</sup> molecular beam epitaxy (MBE),<sup>14</sup> hybrid physical-chemical vapor deposition (HPCVD),<sup>15</sup> sputtering,<sup>16,17</sup> and reactive evaporation.<sup>18</sup> Growth was performed by *in-situ* techniques<sup>14,15,17,18</sup>, as well as *ex-situ* methods with post-annealing in Mg vapor<sup>12,13</sup>. C-doped films were produced by HPCVD<sup>15</sup> with the addition of 75 sccm of  $(\text{C}_5\text{H}_5)_2\text{Mg}$  to the  $\text{H}_2$  carrier gas. Some films were damaged with  $10^{16} \text{ cm}^{-2}$ , 2 MeV  $\alpha$ -particles to controllably alter the scattering by irradiation point defects.<sup>19</sup> Elemental compositions were determined by wavelength dispersive spectroscopy (WDS) and Rutherford Backscattering Spectroscopy (RBS), and film orientation and lattice parameters with a four-circle X-ray diffractometer. Film parameters are summarized in Table I. In some samples RBS detected through-thickness composition variations, likely due to surface reactions

Measurements of  $H_{c2}(T)$  on samples A, B, E, F, H, I, L were performed in a 33T resistive magnet at the NHMFL in Tallahassee. Film resistances  $R(H)$  were measured in parallel and perpendicular fields at a sweep

rate of 1T/min while temperature was stabilized to  $\sim 10$  mK. The measuring current density  $J$  was varied between 10 and 100 A/cm<sup>2</sup>. Detailed study of film A did not show any significant change in  $R(H)$  for  $4 < J < 4000$  A/cm<sup>2</sup>. Samples G, M and N were measured in the 300 msec 60 T pulsed facility at the LNCMP in Toulouse, at a lock-in frequency of 40 KHz and  $J$  varying from 50 to 200 A/cm<sup>2</sup> with no change in  $R(H)$ . In all cases  $H_{c2}$  was defined as  $R(H_{c2}) = 0.9R(T_c)$ .

Figure 1 shows  $H_{c2}^{\perp}(T)$  (a) and  $H_{c2}^{\parallel}(T)$  (b) for the lower  $H_{c2}$  samples A, B, C, E, H, I, L, M, N, for which a wide variety of properties can be developed.  $R(H)$  curves for film A are shown in inset. The  $H_{c2}^{\perp}(T)$  data in Fig. 1a fall into two groups, one having  $T_c \approx 32$ -37K, with relatively low  $dH_{c2}/dT$  and  $H_{c2}(0) \sim 10.5$ -15T, while the lower  $T_c$  group (24–32K) has  $\approx 50\%$  larger  $dH_{c2}/dT$  and  $H_{c2}(0) \sim 17$ –22T.  $H_{c2}(0)^{\parallel}$  data in Fig. 1b range more continuously from 18-40T, with only samples B and L standing out. Film B, with the lowest  $T_c \approx 24$ K and  $H_{c2}(0)$  with  $\rho_n \sim 85 \mu\Omega\text{cm}$ , has almost identical  $H_{c2}^{\parallel}(T)$  and  $H_{c2}^{\perp}(T)$ , while non-textured sample L with  $\rho_n \sim 9.9 \mu\Omega\text{cm}$  also has a low  $H_{c2}(0) \sim 22$ T in spite of its higher  $T_c = 39.4$ K. Film E, with highest  $T_c = 41.5$  K and  $\rho_n \sim 0.4 \mu\Omega\text{cm}$  as made ( $1.6 \mu\Omega\text{cm}$  when measured at the NHMFL) represents  $\text{MgB}_2$  in the clean limit<sup>20</sup>, making it unsuitable for fitting using dirty-limit theory.<sup>8</sup> Although film E has the lowest  $\rho_n$ , it exhibits the highest  $H_{c2}^{\parallel}(T)$ , even though Fig. 1b also includes films with  $\rho_n > 500 \mu\Omega\text{cm}$  but with lower  $H_{c2}^{\parallel}$  (film I). Thus, there is no simple correlation between  $\rho_n$  and  $H_{c2}$ , because the global resistivity may be limited by poor intergrain connectivity<sup>21</sup> while  $H_{c2}$  is controlled by intragrain impurity scattering. The anisotropy parameter  $\gamma(T) = H_{c2}^{\parallel}/H_{c2}^{\perp}$  ranges from  $\approx 3$  for the lowest  $\rho_n$  film (E,  $T_c = 41.5$ K) to  $\approx 1$  for the lowest  $T_c$  textured film B ( $T_c = 24$ K). For most films,  $\gamma(T)$  tends to decrease as  $T$  decreases, consistent with the behavior predicted for two-gap  $\text{MgB}_2$  with dirtier  $\pi$  band<sup>10</sup>.

Figure 2 shows  $H_{c2}^{\parallel}(T)$  and  $H_{c2}^{\perp}(T)$  curves for the highest  $H_{c2}$  films D, F and G, while the insets show the parallel-field  $R(H)$  traces. By increasing the nominal carbon content in the HPCVD films, resistivity rises from  $\sim 1.6$  (E) to 564 (F) and 250  $\mu\Omega\text{cm}$  (G), while  $T_c$  only decreases to 35K. However,  $H_{c2}^{\perp}(0)$  increases from 12T (E) to 28T (G) and  $\approx 40$ T (F). Furthermore,  $H_{c2}^{\parallel}(0)$  rises from  $\approx 35$ T (E) to 51T (G) and more than 70T in sample F, while the anisotropy parameter  $\gamma(T) = H_{c2}^{\parallel}(T)/H_{c2}^{\perp}(T)$  decreases as  $\rho_n$  increases. Figure 2c presents  $H_{c2}(T)$  for sample D, which has high nominal O (17at.%) and C (14at.%) content.<sup>8</sup> Unlike the two *in situ* films made by HPCVD, film D was made *ex situ* by PLD. This film has  $H_{c2}^{\perp}(0) \approx 33$ T and  $H_{c2}^{\parallel}(0) \approx 48$ T.

The  $H_{c2}(T)$  curves in Fig. 2 have an upward curvature inconsistent with the dirty limit one-band theory.<sup>9</sup> For two-gap pairing, intraband scattering does not affect  $T_c$ , but  $T_c$  decreases as the pair-breaking interband scattering parameter  $g = (\Gamma_{\sigma\pi} + \Gamma_{\pi\sigma})\hbar/2\pi k_B T_{c0}$  increases, where  $T_{c0} = T_c(g=0)$ . Due to the orthogonality of the  $\sigma$  and  $\pi$  orbitals in  $MgB_2$ ,  $g$  is usually small, and  $T_c$  does not change much, even if  $\rho_n$  is significantly increased.<sup>25</sup> The insensitivity of  $T_c$  to scattering makes it possible to increase  $H_{c2}$  in  $MgB_2$  to a much greater extent than in one-gap superconductors by optimizing the diffusivity ratio  $D_\pi/D_\sigma$ . The equation for  $H_{c2}$  and  $T_c$  in a dirty two-gap superconductor has the form<sup>10</sup>

$$2w(\ln t + U_+)(\ln t + U_-) + (\lambda_0 + \lambda_i)(\ln t + U_+) + (\lambda_0 - \lambda_i)(\ln t + U_-) = 0, \quad (1)$$

$$\psi\left(\frac{1}{2} + \frac{g}{t_c}\right) - \psi\left(\frac{1}{2}\right) = -\frac{2 \ln t_c (w \ln t_c + \lambda_0)}{2w \ln t_c + \lambda_0 + \lambda_i}, \quad (2)$$

where  $t = T/T_{c0}$ ,  $t_c = T_c/T_{c0}$ ,  $T_{c0} = 1.13\theta_D \exp[-(\lambda_- + \lambda_0)/2w]$ ,  $w = \lambda_{\sigma\sigma}\lambda_{\pi\pi} - \lambda_{\sigma\pi}\lambda_{\pi\sigma}$ ,  $\lambda_0 = (\lambda_-^2 + 4\lambda_{\sigma\pi}\lambda_{\pi\sigma})^{1/2}$ ,  $\lambda_\pm = \lambda_{\sigma\sigma} \pm \lambda_{\pi\pi}$ ,  $\lambda_{mn}$  is  $2 \times 2$  matrix of BCS coupling constants,  $\lambda_{\sigma\sigma}$  and  $\lambda_{\pi\pi}$  describing intraband pairing, and  $\lambda_{\sigma\pi}$  and  $\lambda_{\pi\sigma}$  describing interband pairing. Here  $\lambda_i = [(\omega + \Gamma_-)\lambda_- - 2\lambda_{\sigma\pi}\Gamma_{\pi\sigma} - 2\lambda_{\pi\sigma}\Gamma_{\sigma\pi}]/\Omega_0$ ,  $\Gamma_\pm = \Gamma_{\sigma\pi} \pm \Gamma_{\pi\sigma}$ ,  $\omega_\pm = (D_\sigma \pm D_\pi)\pi H/\phi_0$ ,  $\Omega_0 = (\omega_-^2 + \Gamma_+^2 + 2\Gamma_+\omega_-)^{1/2}$ ,  $U_\pm(H, T) = \psi(1/2 + \hbar\Omega_\pm/2\pi k_B T) - \psi(1/2)$ ,  $\Omega_\pm = \omega_+ + \Gamma_+ \pm \Omega_0$ , where  $\psi(x)$  is the digamma function, and  $\phi_0$  is the flux quantum. For  $\mathbf{H}||ab$ , the diffusivities in Eq. (1) should be replaced according to:  $D \rightarrow [D^{(ab)}D^{(c)}]^{1/2}$ .<sup>10</sup>

The evolution of  $H_{c2}(T)$  and  $T_c$  with  $g$  is shown in Fig. 3. For dirty  $\pi$  band ( $D_\pi \ll D_\sigma$ ) and  $g = 0$ ,  $H_{c2}(T)$  has an upward curvature, because  $dH_{c2}/dT$  at  $T_c$  is determined by the larger  $D_\sigma$ , while  $H_{c2}(0)$  is determined by the smaller  $D_\pi$ . As  $g$  increases, the upward curvature of  $H_{c2}(T)$  diminishes, and  $T_c$  decreases. In the limit  $g \gg 1$  of complete interband mixing,  $T_c(g)$  approaches  $T_{\min} = T_{c0} \exp[-(\lambda_0 + \lambda_i)/2w]$ , while  $H_{c2}(T)$  for fixed  $D_\pi$  and  $D_\sigma$  evolves toward the one-gap  $H_{c2}(T)$  curve. The case of a dirtier  $\sigma$  band,  $D_\pi \gg D_\sigma$  corresponds to a one-gap-like  $H_{c2}(T)$  curve broadened near  $T_c$  by the band mixing.

We used Eqs. (1)-(2) to describe the observed  $H_{c2}(T)$ , taking *ab-initio* values<sup>3</sup>  $\lambda_{\sigma\sigma} = 0.81$ ,  $\lambda_{\pi\pi} = 0.28$ ,  $\lambda_{\sigma\pi} = 0.115$  and  $\lambda_{\pi\sigma} = 0.09$  as input parameters. First,  $g$  was calculated from Eq. (2) with the observed  $T_c$  and  $T_{c0} = 39K$ . Next, we calculated  $D_\sigma$  from the observed (or extrapolated)  $H_{c2}(0)$ , leaving the ratio  $D_\pi/D_\sigma$  as the

only fit parameter determining the shape of  $H_{c2}(T)$ . This procedure is based on a conventional assumption of the dirty limit theory that impurities only change the scattering rates, but do not affect the coupling constants  $\lambda_{mn}$ , or the electron density of states. The fits describe well the observed  $H_{c2}(T)$  curves in Fig. 2, indicating that  $\pi$  scattering is stronger than  $\sigma$  scattering in all our high- $H_{c2}$  films. The extrapolated  $H_{c2}^{\parallel}(0)$  reaches  $\approx 55T$  for film G and  $>70T$  for film F.<sup>26</sup>

Our  $H_{c2}(T)$  data are striking because the highest  $H_{c2}$  values are attained for films with weak  $T_c$  suppressions, and the three highest- $H_{c2}$  films ( $48 < H_{c2}^{\parallel}(0) < 70T$ ) greatly exceed the  $H_{c2}^{\parallel}(0)$  values reported for C-doped  $MgB_2$  single crystals ( $\sim 35T$ )<sup>22,23</sup> and C-doped filaments ( $32T$ ).<sup>24</sup> The fits to  $H_{c2}(T)$  for films D, F, and G, which all have significant C content, indicate much stronger  $\pi$  than  $\sigma$  scattering.

We find that the very broad range of  $\rho_n$  ( $\sim 1-600\mu\Omega\text{cm}$ ) does not directly manifest itself in the atomic-scale scattering that actually determines  $H_{c2}$ , because current-blocking extended defects<sup>21</sup> control the measured resistivity. TEM on a C-doped HPCVD film found significant amorphous C-rich phase and scattered  $MgC_2$  precipitates surround many  $Mg(B_{1-x}C_x)_2$  grains, thus showing that much less than the total C content from Table I is dissolved in  $MgB_2$ . Because  $T_c$  is depressed to zero at  $x \sim 0.15$  ( $\approx 10\%$ ) and  $\rho_n \geq 50\mu\Omega\text{cm}$  in  $Mg(B_{1-x}C_x)_2$  single crystals<sup>22,23</sup> and filaments<sup>24</sup>, this would indicate that films with  $T_c$  of 33-35K have  $x \sim 0.03-0.05$  within the  $MgB_2$  grains. This heterogeneous microstructure results in  $T_c$  inhomogeneities, which manifest themselves in the resistive transition broadening in Figs. 2.

To understand the scattering mechanisms better, we observe that, similar to C-alloyed  $MgB_2$  single crystals,<sup>28</sup> our high- $H_{c2}$  films F and G have smaller  $a$ -axis lattice spacing than the clean limit value of 0.3085nm. However, the  $c$ -axis lattice spacing in our high- $H_{c2}$  films is larger than the value of 0.3524nm measured for bulk pure and C-alloyed single crystals and filaments.<sup>24,28</sup> TEM study of film D showed buckling of the  $ab$  planes<sup>8</sup> (perhaps due to strains induced by as-grown nanophase precipitates), naturally causing the  $c$ -axis lattice expansion. Furthermore, lattice buckling results in strong  $\pi$  scattering due to disturbance of the  $p_z$   $\pi$  orbitals, and thus dirtier  $\pi$  band ( $D_\pi \ll D_\sigma$ ) necessary to account for the upward curvature of  $H_{c2}(T)$  in Figs. 2b and 2c. This scenario may also explain how C (which normally substitutes for B) can result both in the strong in-plane  $\sigma$  band scattering and out-of-plane  $\pi$  scattering required for the observed  $H_{c2}$  enhancement.

In conclusion, we have performed extensive studies of the effect of disorder on  $H_{c2}$  of  $MgB_2$  and report record high  $H_{c2}$  values, which may approach the paramagnetic limit for C-doped films. The upward curvature of  $H_{c2}(T)$  and weak  $T_c$  suppression are described well by the two-gap theory.

Work at UW was supported by NSF under MRSEC grant DMR-0079983, work at Penn State was supported under ONR Nos. N00014-00-1-0294 (Xi) and N0014-01-1-0006 (Redwing), by NSF under grant Nos. DMR-0306746 (Xi and Redwing), DMR-9876266 and DMR-9972973 (Li), and work at Arizona State U was supported under ONR Nos. N00014-02-1-0002. The NHMFL user facility is supported by NSF.

## References

1. A.Y. Liu, I.I. Mazin, and J. Kortus, Phys. Rev. Lett. **87**, 087005 (2001)
2. H.J. Choi, *et al.*, Nature **418**, 758 (2002)
3. A.A. Golubov *et al.*, J. Phys: Condensed Matter., **14**, 1353 (2002); A. Brinkman *et al.*, Phys. Rev. B **65**, R18051 (2002)
4. P.C. Canfield, and G.W. Crabtree, Physics Today, **56**, 34 (2003); P.C. Canfield, S.L. Bud'ko, and D.K. Finnemore, Physica C **385**, 1 (2003)
5. R. Cava, H.W. Zandbergen, and K. Inumare, Physica C **385**, 8 (2003)
6. V.Ferrando *et al.*, Phys. Rev. B **68**, 94517 (2003).
7. F. Bouquet *et al.*, Physica C **385**, 192 (2003).
8. A. Gurevich *et al.*, Supercond. Sci. Technol. **17**, 278 (2004).
9. N.R. Werthamer, E. Helfand, and P.C. Hohenberg, Phys. Rev. **147**, 288 (1966)
10. A. Gurevich, Phys. Rev. B **67**, 184515 (2003).
11. A.A. Golubov and A.E. Koshelev, Phys. Rev. B **68**, 104503 (2003)
12. V. Ferrando, *et al.*, Supercond. Sci. Technol. **16**, 241 (2003)
13. C.B. Eom *et al.*, Nature **411**, 558 (2001)
14. J. Kim, *et al.*, IEEE Trans. Appl. Supercond. **13**, 3238 (2003)
15. X. Zeng *et al.*, Nature Mat. **1**, 35 (2002)
16. S.D. Bu *et al.*, Appl. Phys. Lett. **81**, 1851 (2002)
17. R. Vaglio, M.G. Maglione and R. Di Capua, Supercond. Sci. Technol. **15**, 1236 (2002).
18. B. Moeckly (unpublished).
19. R. Gandikota *et al.*, (unpublished)
20. A.V. Pogrebnyakov *et al.*, Appl. Phys. Lett. **82**, 4319 (2003)
21. J.M. Rowell, Supercond. Sci. Technol. **16**, R17 (2003)
22. T. Masui, S. Lee, and S. Tajima, cond-mat/0312458
23. E. Ohmichi, *et al.*, cond-mat/0312348
24. R.H.T. Wilke *et al.*, cond-mat/0312235

25. I.I. Mazin *et al.*, Phys. Rev. Lett. **89**, 107002 (2002)
26. Given the limited field range in our experiments we used Eqs. (1) and (2) without paramagnetic terms to fit the data. Analysis of paramagnetic effects will be given elsewhere.
27. A. V. Pogrebnyakov *et al.*, (unpublished)
28. S. Lee, *et al.*, Physica C **397**, 7 (2003)



## Figure captions

### Figure 1:

$H_{c2}^{\perp}(T)$  (a) and  $H_{c2}^{\parallel}(T)$  (b) for samples A, B, C, E, H, I, L, M, and N. The lines are guides for the eye. Insets show  $R(H)$  for sample A for:  $T = 2.1, 4.2, 8, 10, 15, 20, 22, 25, 30$  K (a), and  $T = 2.47, 3.34, 4.2, 6.8, 10, 12, 15, 18.2, 20, 22, 25, 28, 32$  K (b). The  $R(H_{c2}) = 0.9R_n$  criterion used to determine  $H_{c2}$  is shown with a dashed line.

### Figure 2:

$H_{c2}^{\parallel}(T)$  (triangles) and  $H_{c2}^{\perp}(T)$  (squares) for films G (a), F (b) and D (c). Insets show the raw  $R(H)$  traces for  $H||ab$ . Solid curves are calculated from Eqs. (1) and (2) with fit parameters given in Table I.

### Figure 3:

$H_{c2}(T)$  curves calculated from Eq. (1) for  $D_{\pi} = 0.03D_{\sigma}$  and  $g = 0.01, 0.05, 0.2, 1, 10$  (from top to bottom). Inset shows  $T_c(g)$  calculated from Eq. (2) with  $\lambda_{mn}$  taken from Ref. 3.

**Table I**

Samples	Substrate	T <sub>c</sub> (K)	ρ <sub>n</sub> (40K) (μΩcm)	H <sub>c2</sub> <sup>⊥</sup> (T)	H <sub>c2</sub> <sup>∥</sup> (T)	g	D <sub>π</sub> /D <sub>σ</sub>	c (Å)	a (Å)	Mg at%	B at%	C at%	O at%
A epitaxial <sup>16</sup>	(0001)Al <sub>2</sub> O <sub>3</sub>	35	9(4)	13.5	33	0.045	0.12	3.516	3.047	29	53	10	8
B fiber-textured <sup>16</sup>	(0001)Al <sub>2</sub> O <sub>3</sub>	23.7	86(56)	17	17	0.5	<<1	-	-	28	57	7	8
C epitaxial* <sup>16</sup>	(0001)Al <sub>2</sub> O <sub>3</sub>	34	7	20.5	30	0.06	<<1	3.52	3.08	-	-	-	-
D fiber-textured* <sup>13</sup>	(111)SrTiO <sub>3</sub>	31	220	33	48	0.075	<<1	3.547	-	37	32	14	17
E epitaxial	SiC	41.5	1.6(0.4)	12	34.5	-	-	3.511	3.107	30	57	2	11
F fiber-textured <sup>15</sup>	SiC	35	564	40	>74	0.045	<<1	3.542	3.055	26	46	21	6
G fiber-textured <sup>15</sup>	SiC	35	250	28.2	55.5	0.045	0.065	3.536	3.057	25	42	26	6
H epitaxial <sup>15</sup>	SiC	38	10.5	10.5	30	0.025	0.06	3.519	3.107	31	63	4	1
I untextured <sup>14</sup>	(0001)Al <sub>2</sub> O <sub>3</sub>	32	567(290)	21.7	26.8	0.09	0.08	-	-	-	-	-	-
L no 00l textured <sup>18</sup>	r-cut Al <sub>2</sub> O <sub>3</sub>	39.4	9.9(2.8)	10.8	21.4	0.025	0.07	-	-	32	65	1	1
M epitaxial <sup>12</sup>	(111)MgO	33.5	47	14.6	38.1	0.095	0.1	3.533	3.036	24	41	28	6
N untextured <sup>17</sup>	(001)MgO	28.6	400	15.8	24.3	0.155	<<1	-	-	33	53	5	9

Sample list with substrate, texture and lattice parameters derived from XRD and chemical compositions deduced from WDS. Impurities detected in amounts less than 1 at.% are not listed. ρ<sub>n</sub>(40K) was obtained during H<sub>c2</sub> measurements (as-grown values are given in parentheses). H<sub>c2</sub><sup>∥</sup> and H<sub>c2</sub><sup>⊥</sup> values were extrapolated to 0K, and g and D<sub>π</sub>/D<sub>σ</sub> were deduced from the fit of H<sub>c2</sub>(T) curves for all films. (D<sub>π</sub>/D<sub>σ</sub> << 1 means that the data point scatter does not allow us to distinguish between finite and zero D<sub>π</sub>/D<sub>σ</sub>, so the fit was performed for D<sub>π</sub> = 0).

Figure 1 a

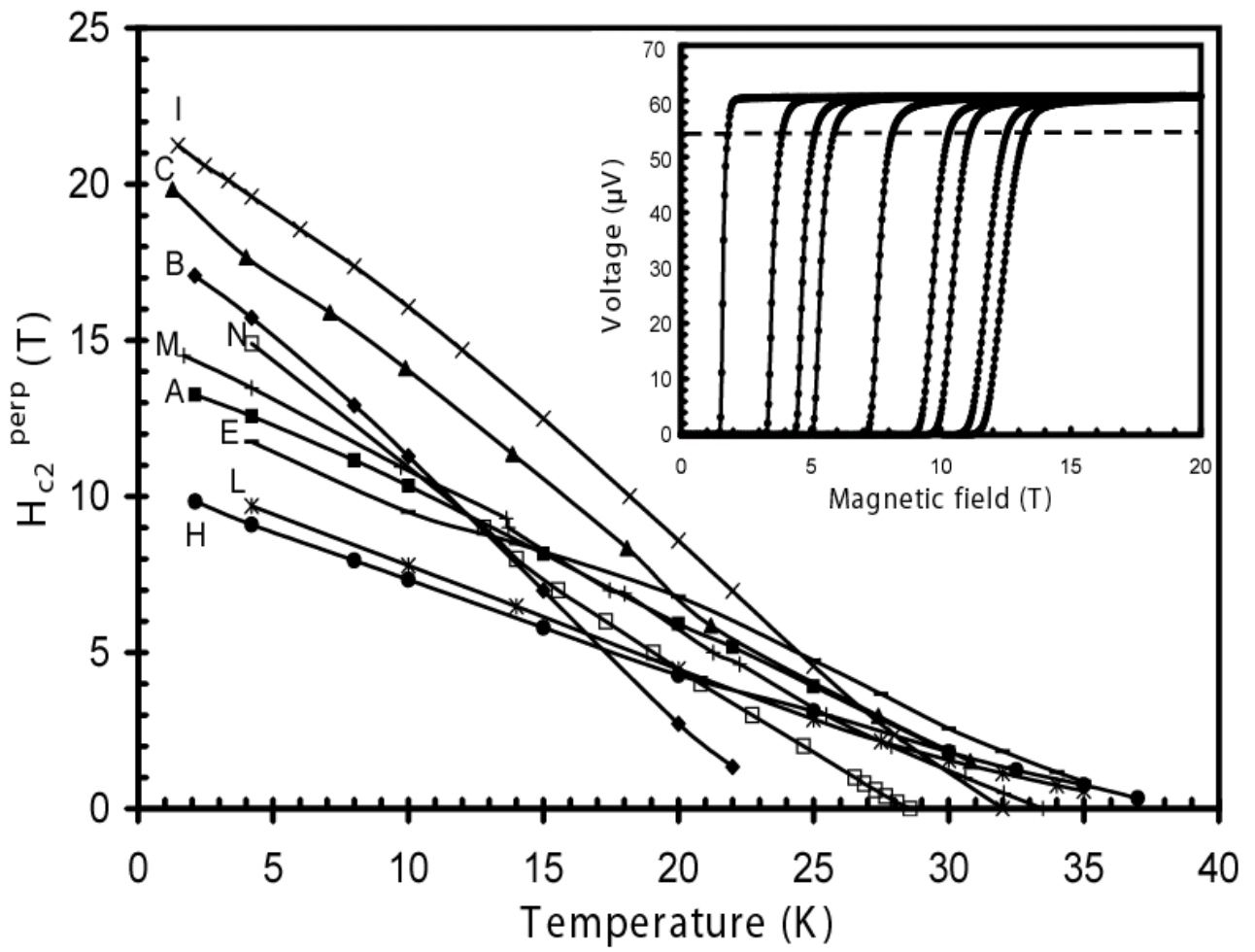


Figure 1 b

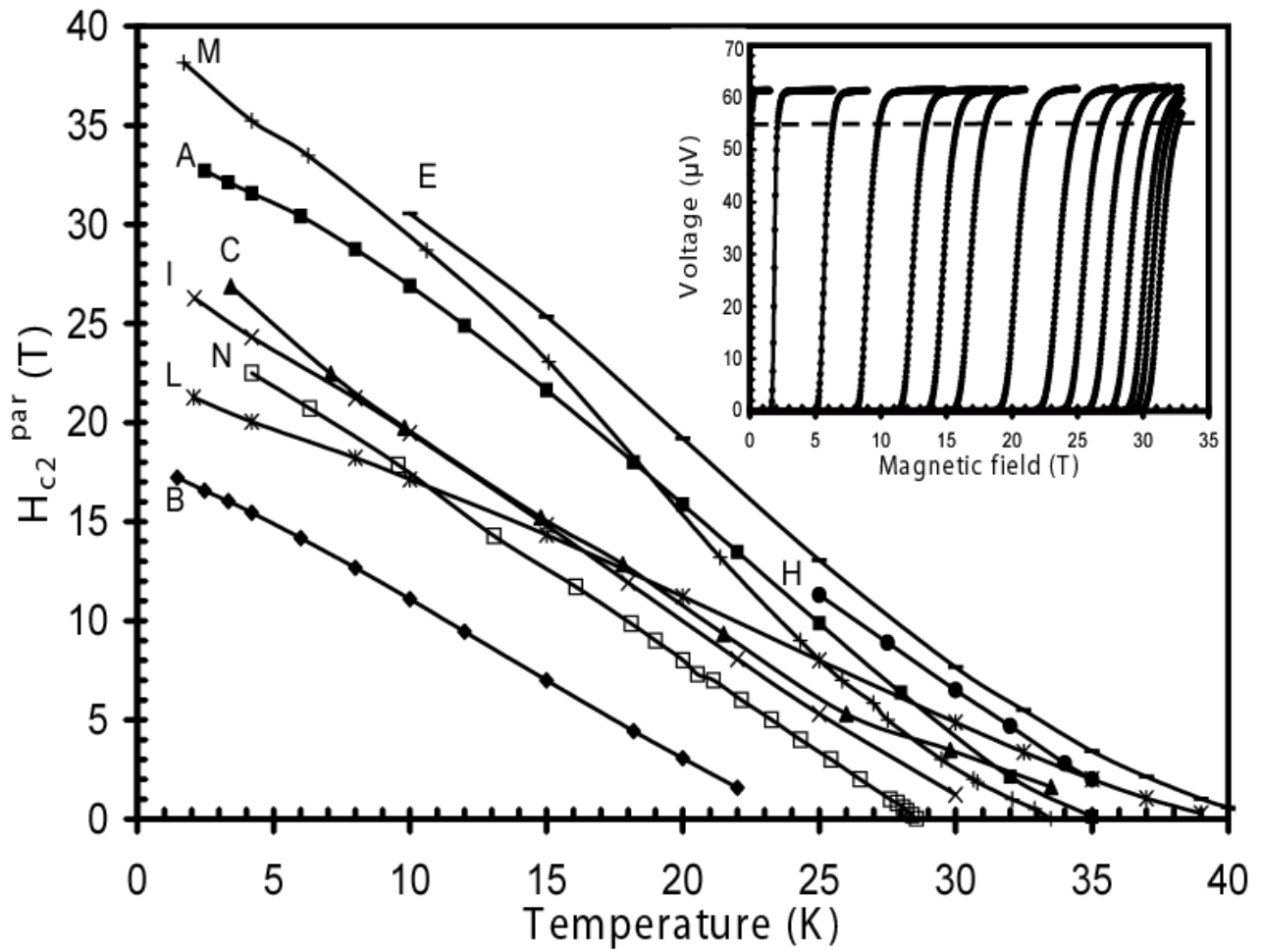


Figure 2 a

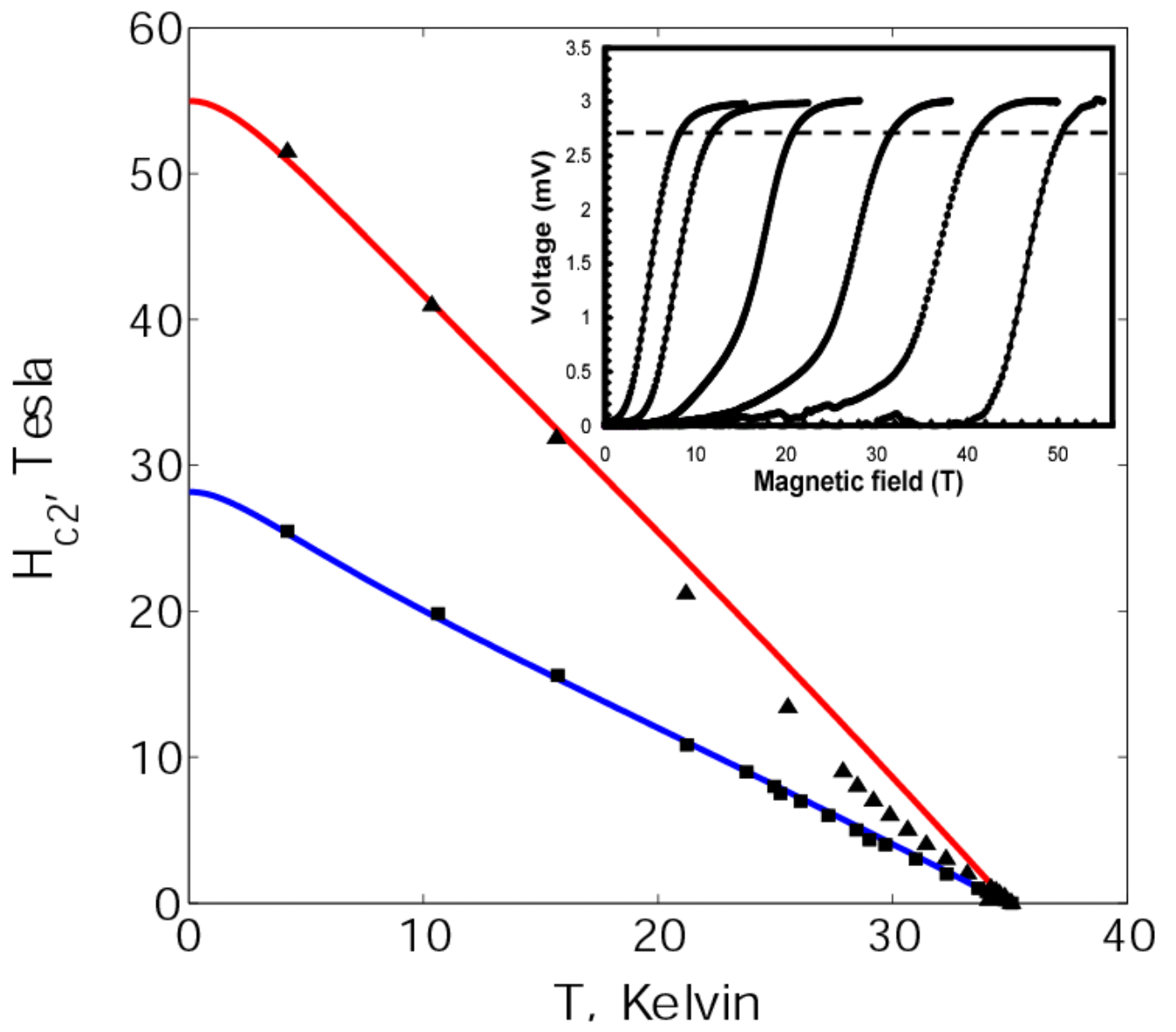


Figure 2 b

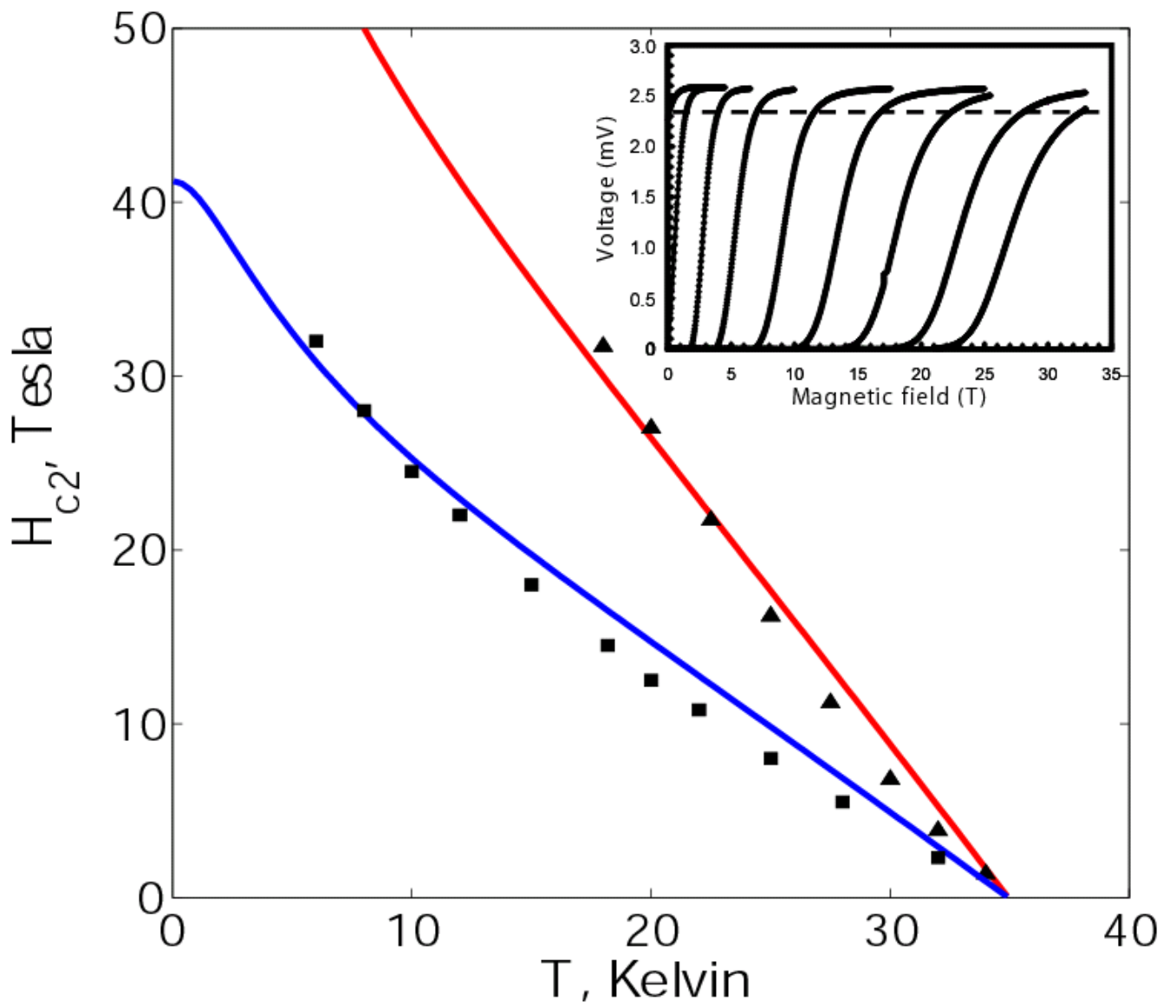


Figure 2 c

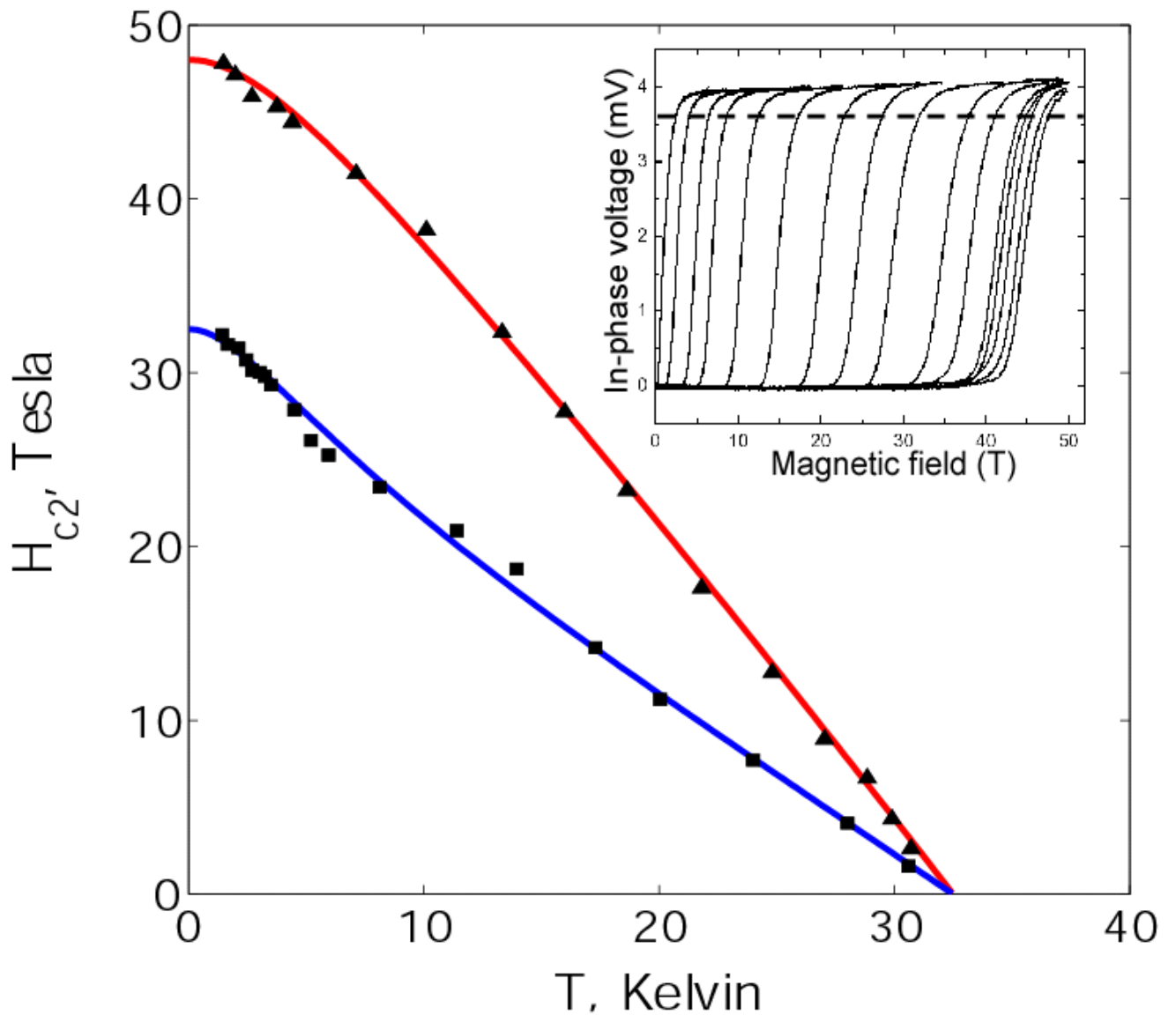


Figure 3

